JCI insight

Heterogeneous perivascular cell coverage affects breast cancer metastasis and response to chemotherapy

Jiha Kim, … , Funda Meric-Bernstam, Valerie S. LeBleu

Research Article   **Angiogenesis**   **Vascular biology**

Angiogenesis and co-optive vascular remodeling are prerequisites of solid tumor growth. Vascular heterogeneity, notably perivascular composition, may play a critical role in determining the rate of cancer progression. The contribution of vascular pericyte heterogeneity to cancer progression and therapy response is unknown. Here, we show that angiopoietin-2 (Ang2) orchestrates pericyte heterogeneity in breast cancer with an effect on metastatic disease and response to chemotherapy. Using multispectral imaging of human breast tumor specimens, we report that perivascular composition, as defined by the ratio of PDGFRβ$^-$ and desmin$^+$ pericytes, provides information about the response to epirubicin but not paclitaxel. Using 17 distinct patient-derived breast cancer xenografts, we demonstrate a cancer cell–derived influence on stromal Ang2 production and a cancer cell–defined control over tumor vasculature and perivascular heterogeneity. The aggressive features of tumors and their distinct response to therapies may thus emerge by the cancer cell–defined engagement of distinct and heterogeneous angiogenic programs.

Find the latest version:

https://jci.me/90733/pdf

JCI iNSIGHT

Heterogeneous perivascular cell coverage affects breast cancer metastasis and response to chemotherapy

Jiha Kim,[1] Pedro Correa de Sampaio,[1] Donna Marie Lundy,[1] Qian Peng,[1] Kurt W. Evans,[2] Hikaru Sugimoto,[1] Mihai Gagea,[3] Yvonne Kienast,[4] Nayra Soares do Amaral,[5] Rafael Malagoli Rocha,[6] Hans Petter Eikesdal,[7,8] Per Eystein Lønning,[7,8] Funda Meric-Bernstam,[2,9] and Valerie S. LeBleu[1]

[1]Department of Cancer Biology, [2]Department of Investigational Cancer Therapeutics, and [3]Department of Veterinary Medicine and Surgery, University of Texas MD Anderson Cancer Center, Houston, Texas, USA. [4]Discovery Oncology, Roche Pharmaceutical Research and Early Development, (pRED), Roche Innovation Center, Munich, Germany. [5]Department of Anatomic Pathology, AC Camargo Cancer Center, São Paulo, Brazil. [6]Molecular Gynecology Laboratory, Gynecology Department, Federal University of São Paulo, Brazil. [7]Section of Oncology, Department of Clinical Science, University of Bergen, Bergen, Norway. [8]Department of Oncology, Haukeland University Hospital, Bergen, Norway. [9]Department of Breast Surgical Oncology, University of Texas MD Anderson Cancer Center, Houston, Texas, USA.

Angiogenesis and co-optive vascular remodeling are prerequisites of solid tumor growth. Vascular heterogeneity, notably perivascular composition, may play a critical role in determining the rate of cancer progression. The contribution of vascular pericyte heterogeneity to cancer progression and therapy response is unknown. Here, we show that angiopoietin-2 (Ang2) orchestrates pericyte heterogeneity in breast cancer with an effect on metastatic disease and response to chemotherapy. Using multispectral imaging of human breast tumor specimens, we report that perivascular composition, as defined by the ratio of PDGFRβ$^-$ and desmin$^+$ pericytes, provides information about the response to epirubicin but not paclitaxel. Using 17 distinct patient-derived breast cancer xenografts, we demonstrate a cancer cell–derived influence on stromal Ang2 production and a cancer cell–defined control over tumor vasculature and perivascular heterogeneity. The aggressive features of tumors and their distinct response to therapies may thus emerge by the cancer cell–defined engagement of distinct and heterogeneous angiogenic programs.

Introduction

Blood vessels in breast cancer present with perfusion defects associated with vessel dilation, tortuosity, and poor perivascular coverage (1–3). The heterogeneity in the endothelial morphology, permeability, and molecular signatures in human and murine mammary tumors (4–6) has highlighted features of tumor angiogenic programs that are under a complex, microenvironment-driven control, in part mediated by pericyte involvement in the tumor vascular bed (7–12). Defining the regulatory elements that modulate the perivascular-endothelial network to control vessel maturation may offer insights into the clinical response to direct and indirect inhibitors of angiogenesis and unravel antagonistic or synergistic effects of drug combination for the treatment of breast cancer (13–15). Much like cancer cells themselves, the rich microenvironment of breast tumors is highly dynamic and heterogeneous. While pericytes emerge as critical regulators of breast cancer metastasis (3, 9, 10, 16, 17), the impact of their heterogeneous composition on breast cancer metastasis and response to chemotherapy is largely unknown. At the core of perivascular-endothelial cell communication, the angiopoietin signaling network, engaging angiopoietin-1 (Ang1) and angiopoietin-2 (Ang2) mediated signaling, offers a microenvironmental context-dependent regulation of perivascular recruitment (18–21).

Ang2 is a secreted glycoprotein with potent regulatory functions on vascular development, remodeling, and maturation (18, 21). Ang2 signaling is context dependent, engaging distinct autocrine and paracrine signaling pathways, as directed in part by receptor availability and abundance (19, 20, 22, 23). Ang2 is, in part, transcriptionally induced by prototypical angiogenic factors, including VEGFA, PDGF, TNF-α, as

well as decreased oxygen levels (hypoxia), thus partaking in the continuous angiogenic signaling associated with pathological vascular remodeling, including the neovasculature of malignant tumors (18, 19). Enhanced Ang2 signaling in murine breast cancer is also associated with increased brain and lung metastasis (16, 24, 25) and adaptive tumor resistance to VEGF signaling blockade (26). In patients with breast cancer, Ang2 expression in tumors is associated with lymph node involvement and poor prognosis (27) and serum Ang2 levels present with diagnostic and prognostic potential for human breast cancer (28). Ang2 is implicated in the metastasis of breast cancer (16, 24, 29–32) and emerges as an attractive therapeutic target for breast cancer metastasis (33). However, the complex signaling of Ang2 in the tumor microenvironment and its pleiotropic effect on endothelial cells and perivascular cells may limit the efficacy and response to Ang2-targeted therapies, requiring a deeper understanding of the effect of the Ang2 signaling network on vascular remodeling and cancer cell behavior.

We and others have specifically implicated Ang2 in endothelial and perivascular control of metastasis (16, 29, 31, 34, 35). Suppression of Ang2-mediated signaling in PDGFRβ+ cell-depleted murine tumors enabled the control of vascular permeability via the emergence of mature desmin+ perivascular coverage (16). While deregulated Ang2 signaling in breast tumor angiogenesis in part drives the formation of highly abnormal vessels with structural defects, the influence of remodeling the intrinsic and heterogeneous perivascular distribution in breast cancer remains poorly defined. The heterogeneous composition of distinct pericytes, defined by gene products such as desmin, PDGFRβ, NG2, and αSMA, and their specific effect on the breast tumor vasculature has not been characterized, due in part to the inherent experimental challenge associated with resolving the pericyte complexity. Such complex heterogeneous pericyte coverage of the breast tumor vasculature is, however, posited to emerge via cancer intrinsic properties to co-opt their microenvironment and via exogenous cues, such as therapeutic agents, that directly or indirectly affect vascular remodeling. In this study, we deciphered the precise role of perivascular heterogeneity in breast tumors and revealed an unexpected predictive value for defined perivascular score and patient response to a specific chemotherapeutic regimen, epirubicin. In contrast, this perivascular score failed to predict response to paclitaxel. Our results identify a critical and distinct cooperation of cancer cells, and their associated perivascular heterogeneous coverage, in influencing response to chemotherapeutic agents with an effect on patient survival. Our studies using mouse xenografts indicated that a perivascular score that reflected the vascular remodeling program was associated with enhanced metastasis. Furthermore, our studies employing patient-derived xenografts (PDXs) in syngeneic recipient mice unexpectedly revealed that distinct cancer cell populations, from distinct PDXs, differentially elicited host transcriptional activation of Ang2, dictating the perivascular composition of the growing tumors.

Results

Subtypes of breast cancer exhibit pericyte heterogeneity. Patients with triple-negative breast cancer (TNBC) may present with higher microvascular density (MVD), which possibly enhances their response to neoadjuvant anti-VEGF/bevacizumab therapy, which targets immature and newly formed blood vessels (36). However, the heterogeneous perivascular composition in subtypes of breast cancer remains undefined. We set out to characterize microvessel pericyte coverage index (MPI), perivascular heterogeneity, and MVD in tissue microarrays (TMAs) constructed using resected tumors of patients with TNBC (*n* = 28; *n* = 7 treatment-naive) and luminal breast cancer (luminal A; *n* = 56, luminal B; *n* = 1; *n* = 16 of 57 treatment-naive) tumors (cohort 1, Supplemental Table 1; supplemental material available online with this article; doi:10.1172/jci.insight.90733DS1). We specifically queried the presence of desmin+ and PDGFRβ+ pericytes in proximal relation to CD31+ blood vessels in order to define the perivascular heterogeneity in each of these tumors. To this end, we developed an automated phenotyping algorithm to identify the perivascular coverage of CD31+ blood vessels. Using a multiplex immunohistochemistry technique coupled with Tyramide Signal Amplification, we labeled each TMA slide for CD31, PDGFRβ, desmin, and DAPI (cell nucleus). Multispectral scanning enabled the generation of composite images, which were subsequently used for segmentation analyses (Figure 1A and Supplemental Figure 1, A and B). The segmentation defined perivascular areas as areas containing no more than two nuclei directly adjacent to the CD31+ cells (Figure 1A). By strictly including these perivascular zones or segments for further phenotyping analysis, we effectively excluded all other nonperivascular mesenchymal cells expressing desmin or PDGFRβ, such as fibroblasts and possibly perivascular progenitors not yet associated with blood vessels. Within these perivascular segments, cells that were positive for either one or both pericyte markers were distinctly defined, namely

as PDGFRβ−desmin+, PDGFRβ+desmin−, and PDGFRβ+desmin+ pericytes (Figure 1A and Supplemental Figure 1, A and B). While TNBC patients showed significantly higher MVD when compared with patients with luminal breast cancer (Figure 1B), which is in agreement with previous reports (36), the total pericyte coverage (MPI), encompassing all combinations of pericyte phenotypes (PDGFRβ−desmin+, PDGFRβ+desmin− and PDGFRβ+desmin+), was significantly lower in TNBC patients (Figure 1C), thus indicating that a higher proportion of vessels in TNBC are immature with diminished pericyte coverage. Within each patient tumor evaluated, the MPI did not reflect a bias with respect to MVD, indicating that the computed pericyte coverage adequately reflects the heterogeneous composition of perivascular cells rather than reflecting overall low MVD (Supplemental Figure 1, C–F). Our results revealed that the majority of pericytes in TNBC patients were PDGFRβ+desmin− (Figure 1D), whereas double-positive pericytes (PDGFRβ+desmin+) were the dominant pericyte population in luminal breast cancer patients, followed by PDGFRβ−desmin+ pericytes (Figure 1E). Quantitative analyses support that triple-negative tumors display significantly lower PDGFRβ−desmin+ and PDGFRβ+desmin+ pericyte coverage, and higher PDGFRβ+desmin− pericyte coverage, than luminal tumors (Figure 1, F–I). The TNBC subtype is generally associated with a poor clinical outcome, and we have previously reported that a higher desmin+ pericyte coverage is associated with vessel stability and reduced lung metastasis (16). The perivascular composition and associated phenotypic features of tumor blood vessels reported here hence offer a tumor microenvironmental definition to further differentiate between TNBC and luminal breast cancers. Breast cancer subtypes may thus also attain their characteristics, including aggressive neoplastic behavior and distinct response to specific therapies, by differentially engaging their microenvironment, including the stimulation and generation of unique angiogenic programs with functional effect on disease progression and metastatic dissemination.

Distinct pericyte coverage correlates with the response to chemotherapeutic agents. The first cohort of breast cancer patients studied herein (Figure 1 and Supplemental Table 1) includes specimens collected from both treatment-naive patients and patients after therapy, including various chemotherapy regimens. To define the naive perivascular heterogeneity in breast cancer, we next phenotyped the perivascular composition of tumors collected from breast cancer patients prior to neoadjuvant chemotherapy (Norwegian EpiTax trial, referred to as cohort 2 herein, Supplemental Table 2). A total of 223 patients were included in the Norwegian EpiTax trial (37–39), and TMAs were constructed to represent breast cancer biopsies that were collected prior to initiation of chemotherapy. Treatment-naive patients with locally advanced breast cancer were randomized to either epirubicin or paclitaxel monotherapy. If there was no objective response on this first regimen (20 patients with progressive disease and 54 patients with stable disease), patients were switched to the opposite regimen. TMA cores from 144 of 223 patients were available for this study. TMA samples were stained and analyzed as described above (Figure 1A; Supplemental Figure 1, A and B; and Supplemental Figure 2A). Notably, the distinct difference in MPI and MVD between TNBC and non-TNBC patients in this cohort recapitulated the observation in cohort 1 (Supplemental Figure 2B), yet no significant differences in disease-specific and relapse-free survival were observed between these groups (Supplemental Figure 2C). We segregated patients in cohort 2 into the following subgroups (Supplemental Table 3): (a) epirubicin monotherapy ($n = 51$), (b) paclitaxel monotherapy ($n = 42$), (c) epirubicin, followed by paclitaxel ($n = 23$), and (d) paclitaxel, followed by epirubicin ($n = 28$). Across the different groups, we did not observe any significant differences in disease-specific survival, relapse-free survival, distant metastasis, and tumor size (Supplemental Table 3 and Supplemental Figure 2D). Patients were further categorized based on MPI (high and low) as well as based on the specific nature of the pericyte coverage, namely PDGFRβ+ or desmin+ pericyte coverage (Figure 2A and Supplemental Figure 2A). We defined relative coverage of PDGFRβ+ versus desmin+ pericytes by expressing the ratio of PDGFRβ−desmin+ perivascular counts to the PDGFRβ+desmin− perivascular counts. As such, a high ratio would define desmin-rich perivascular coverage, whereas a low ratio would define PDGFRβ+-rich perivascular coverage. The median of the resultant desmin+/PDGFRβ+ ratio was used as a cutoff to distinguish tumors with high versus low desmin+/PDGFRβ+ ratios (Supplemental Table 3). There was no significant difference in disease-specific and relapse-free survival when all patients were stratified based on high and low desmin+/PDGFRβ+ ratio (Figure 2, B and C); however, there was a significant difference in both disease-specific and relapse-free survival of patients who received epirubicin monotherapy, with improved survival of patients with high desmin+/PDGFRβ+ ratios (Figure 2, D and E). In contrast, there was no significant difference based on the desmin+/PDGFRβ+ ratio in both disease-specific and relapse-free survival of patients that received paclitaxel monotherapy (Figure 2, F and G). Importantly, there was no bias in the overall distribution of
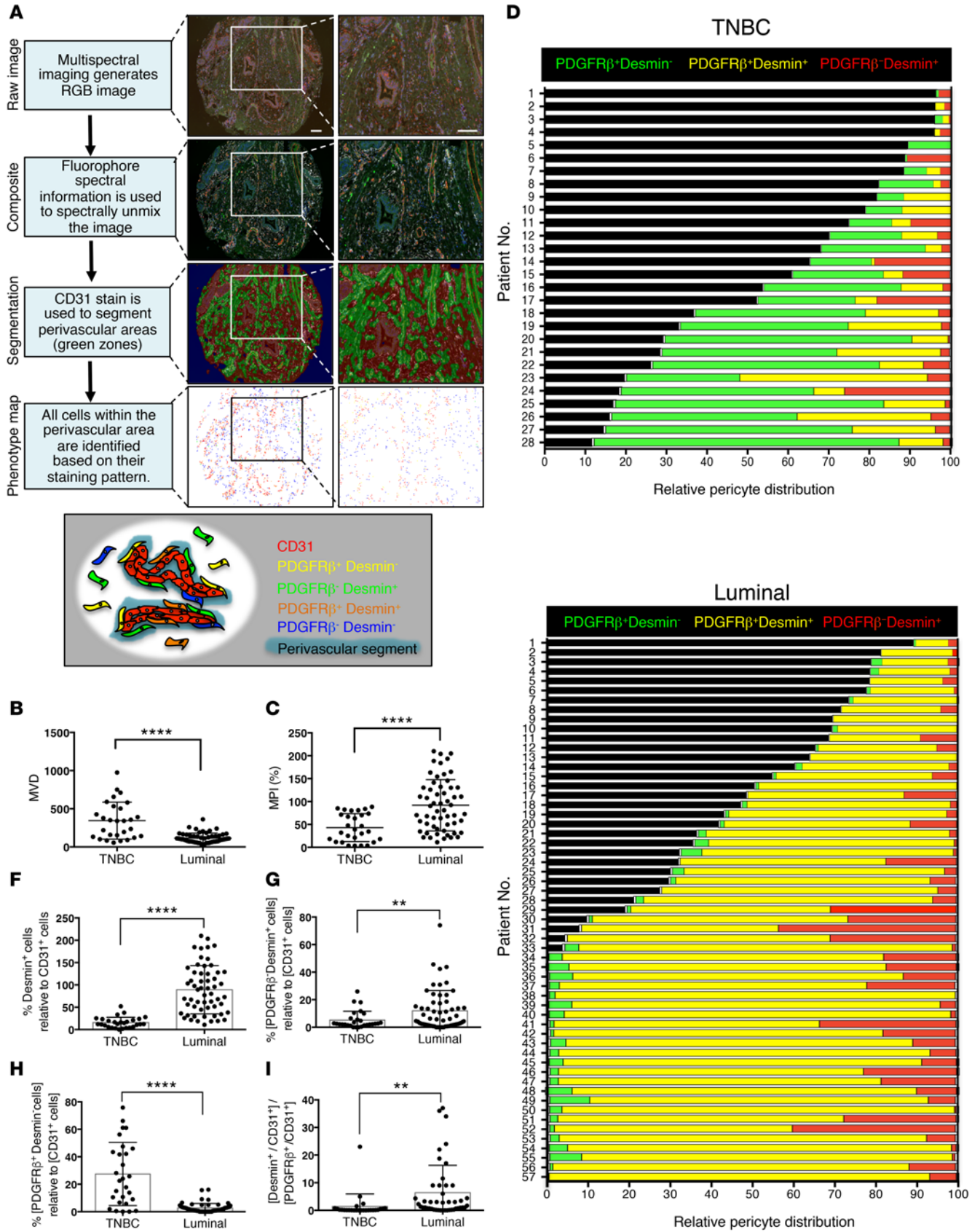
Figure 1. Triple-negative and luminal breast cancer subtypes present distinct pericyte coverage. (**A**) Flow chart highlighting the different steps of the phenotyping analysis of multispectral image cubes using the InForm image analysis software. RGB multispectral images are spectrally unmixed into their different fluorescent components and segmented in three image regions based on the CD31 and DAPI staining patterns: blank (blue), perivascular

(green), and other (red). Individual cells within the perivascular region were identified based on their DAPI staining and assigned 1 of 5 individual phenotypes based on their shape and staining pattern. The phenotype map highlights the different phenotypes identified within the perivascular regions of this particular core. The schematic illustration (bottom) shows different potential phenotypes identified in perivascular regions based on the expression patterns of CD31, desmin, and PDGFRβ. Scale bars: 100 μm. (**B** and **C**) Quantification of CD31$^+$ vascular coverage (microvascular density [MVD]) (**B**) and pericyte coverage index (microvessel pericyte coverage index [MPI]) (**C**) in the indicated patient groups. (**D** and **E**) Relative pericyte distribution of individual patients in the triple-negative breast cancer (TNBC) group (**D**) and the luminal breast cancer group (**E**). Black bars indicate the percentage of vessels not covered by any type of pericyte analyzed (naked vessels). (**F**) Quantification of the percentage of coverage of all desmin$^+$ pericytes (PDGFRβ$^-$desmin$^+$ and PDGFRβ$^+$desmin$^+$) related to CD31$^+$ vessels. (**G**) Quantification of the percentage of coverage of PDGFRβ$^-$desmin$^+$ pericytes related to CD31$^+$ vessels. (**H**) Quantification of the percentage of coverage of PDGFRβ$^+$desmin$^-$ pericytes related to CD31$^+$ vessels. (**I**) Quantification of the ratio of PDGFRβ$^-$ desmin$^+$ pericytes/PDGFRβ$^+$ desmin$^-$ pericytes. TNBC, $n = 26$; luminal, $n = 45$. The data are presented as mean ± SD. Unpaired 2-tailed t test was used to determine statistical significance. **$P < 0.01$, ****$P < 0.0001$. Unless otherwise indicated, TNBC, $n = 28$; luminal, $n = 57$.

desmin$^+$/PDGFRβ$^+$ ratios when comparing all patients, patients with epirubicin monotherapy, and patients with paclitaxel monotherapy (Supplemental Figure 2E), indicating that the differences in patient outcome within each therapy group reflect a segregation of patients based on distinct perivascular coverage rather than a skewed perivascular coverage in that particular group. No significant difference in survival of patients, based on their desmin$^+$/PDGFRβ$^+$ ratios, was observed for any other groups (Supplemental Figure 2, F and G). Taken together, these results indicate that the desmin$^+$/PDGFRβ$^+$ ratio correlates with patient outcome for those receiving epirubicin neoadjuvant therapy but failed to do so for those receiving paclitaxel. Furthermore, these analyses suggest that tumor microenvironmental markers, specifically the markers used here to ascertain perivascular heterogeneity, could indicate the response to a particular chemotherapy regimen.

Ang2 controls perivascular heterogeneity with an effect on lung metastasis in a breast cancer xenograft. To define the effect of perivascular heterogeneity and the desmin$^+$/PDGFRβ$^+$ ratio on metastatic disease, we utilized the MDA-MB-231 orthotopic tumor model and subjected tumors to different agents known to influence perivascular coverage with an effect on metastasis, namely imatinib and sunitinib. Our previous studies implicated these agents, as well as Ang2, in perivascular remodeling with an effect on pulmonary metastasis (16). Furthermore, we also employed neutralization of Ang2 in these experiments to further define the effect of desmin$^+$/PDGFRβ$^+$ ratios on metastasis and implicate Ang2 as a regulatory signaling molecule in the control of perivascular heterogeneity in this model. In orthotopically implanted MDA-MB-231 tumors, the tyrosine kinase inhibitor sunitinib suppressed primary tumor burden (Supplemental Figure 3, A and C). However, when compared with control groups, pulmonary metastases were significantly increased in mice treated with either sunitinib or imatinib, with an elevated number of surface lung nodules and increased percentage of metastatic areas evaluated by histological analyses (Figure 3A and Supplemental Figure 3D). Concurrent treatment with anti-Ang2–neutralizing antibodies synergized with imatinib to reduce primary tumor burden when compared with mice receiving imatinib with isotype control antibodies, or anti-Ang2 alone, or saline with isotype control antibodies (Supplemental Figure 3, A–C). In sunitinib- or imatinib-treated mice, the concurrent therapy with anti-Ang2 antibodies resulted in the control of both primary tumor burden and metastatic disease burden (Figure 3A and Supplemental Figure 3, A–D). This is further exemplified by the distribution of mice on the basis of both primary tumor volume and percentage of metastatic area, wherein mice receiving the therapy regimen that included anti-Ang2 treatment clustered among those with smallest primary and secondary disease burden (Figure 3B). Neutralization of Ang2, as well as treatment of mice with sunitinib alone, enhanced tumor necrosis (Supplemental Figure 3, E and F) in concordance with previous reports describing the increased tumor necrosis observed in mice receiving these antibodies (16, 40). Notably, imatinib and sunitinib treatment alone resulted in elevated levels of circulating Ang2 (Supplemental Figure 3G). This is in agreement with the anticipated transcriptional upregulation of *Angpt2* in hypoxic tumors (16) and elevated levels of serum Ang2 in breast cancer patients with poorer outcomes (28). The anti-Ang2–neutralizing antibodies also appeared to enhance the detection of Ang2 in circulation by ELISA (Supplemental Figure 3H).

The definition of desmin$^+$/PDGFRβ$^+$ ratios in these tumors and association with primary tumor burden and metastatic readout were determined by immunolabeling. Both imatinib and sunitinib can target PDGFRβ signaling with an effect on breast cancer metastasis in mice (3), and we indeed noted that both desmin$^+$ and PDGFRβ$^+$ pericyte coverage was decreased in tumors of mice treated with imatinib or sunitinib. However, additional treatment with anti-Ang2 antibodies restored pericyte coverage (Figure 3, C–E, and Supplemental Figure 4, A and B). Our results also highlighted that decreased pericyte coverage in the primary
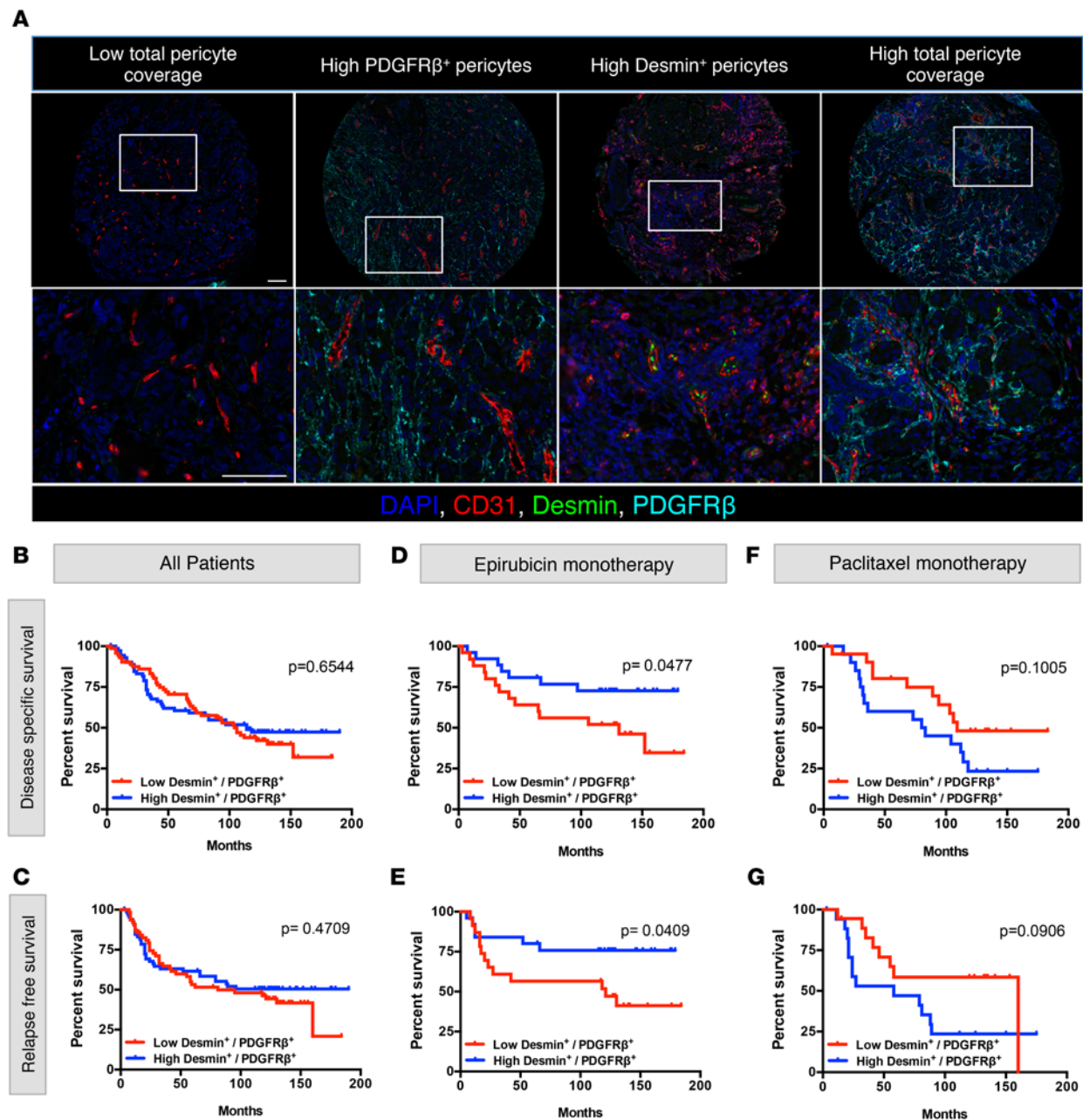
Figure 2. Specific perivascular composition correlates with the outcome of epirubicin-treated breast cancer patients. (**A**) Representative multi-spectral images of multiplex stained tissue microarray sections, displaying differential pericyte coverage levels. Enlarged images are provided for each core. Scale bars: 100 μm. Images on the bottom row are higher-magnification images of boxed areas shown in the top row. (**B** and **C**) Disease-specific survival (**B**) and relapse-free survival (**C**) analysis of all breast cancer patients in cohort 2, stratified based on the pericyte PDGFRβ⁻ desmin⁺/PDGFRβ⁺ desmin⁻ ratio. (**D** and **E**) Disease-specific survival (**D**) and relapse-free survival (**E**) analysis of patients who received epirubicin monotherapy, stratified on the same ratio of PDGFRβ⁻desmin⁺/PDGFRβ⁺desmin⁻ pericyte coverage. (**F** and **G**) Disease-specific survival (**F**) and relapse-free survival (**G**) analysis of patients who received paclitaxel monotherapy, stratified on the same ratio of PDGFRβ⁻desmin⁺/PDGFRβ⁺desmin⁻ pericyte coverage. For disease-specific survival analysis, total number of patients, n = 144; epirubicin monotherapy, n = 51; paclitaxel monotherapy, n = 42. For relapse-free survival analysis, total number of patients, n = 129; epirubicin monotherapy, n = 48; paclitaxel monotherapy, n = 36. Log-rank test was used to determine statistical significance.

tumor, similarly in both imatinib- and sunitinib-treated mice (Figure 3D), rather than changes in primary tumor burden, was associated with the enhanced and similar metastatic disease burden observed in imatinib- and sunitinib-treated mice (Figure 3A). While tumor vascular leakage, measured by tumor interstitial accumulation of systemically administered FITC-dextran, was enhanced in MDA-MB-231 tumors treated with imatinib or sunitinib, such vascular damage was significantly restored with anti-Ang2 therapy (Figure
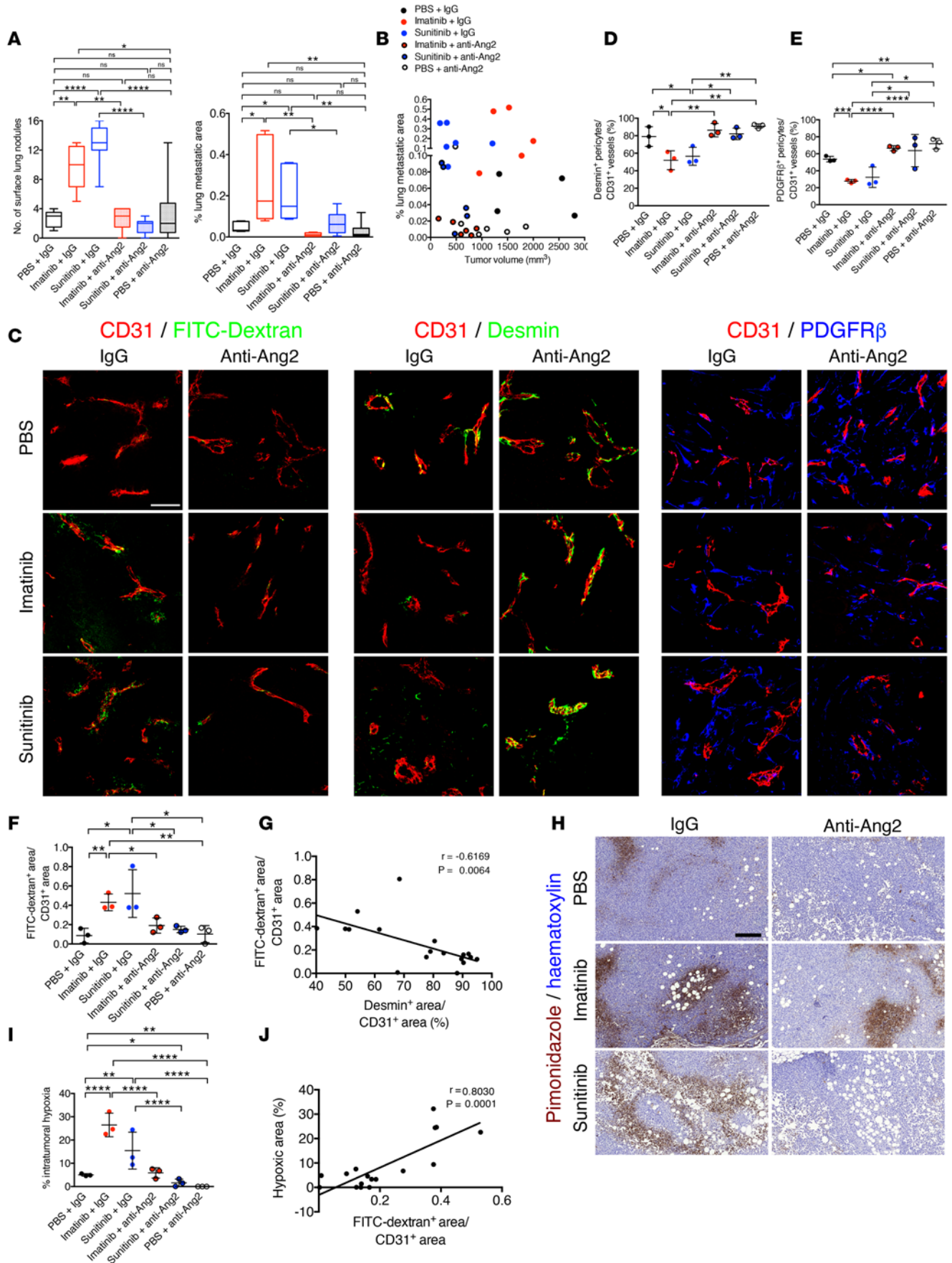
Figure 3. Perivascular composition demarcates metastatic burden in MDA-MB-231 tumor-bearing mice. (**A**) Number of surface lung nodules and quantification of percentage of lung metastatic area determined on H&E-stained lung sections (Supplemental Figure 3D). Box-and-whiskers plots show median (line within box), upper and lower quartile (bounds of box), and minimum and maximum values (bars). (**B**) Correlation of percentage of lung metastasis and tumor volume at experimental endpoint. Experimental n numbers for **A** and **B** were as follows: IgG + PBS, $n = 5$; IgG + imatinib, $n = 5$; anti-ANG2 + imatinib, $n = 6$; anti-ANG2 + PBS, $n = 6$; IgG + sunitinib, $n = 7$; anti-ANG2 + sunitinib, $n = 6$. (**C**) Representative images of FFPE tumor sections from the indicated experimental groups immunolabeled for CD31/FITC-dextran, CD31/desmin, or CD31/PDGFRβ. Tumor sections were visualized for perfused 2,000-kDa FITC-dextran in the indicated experimental groups. Scale bar: 50 μm. (**D**) Quantification of percentage of coverage of desmin+ pericytes per CD31+ vessels ($n = 3$ mice, all groups). (**E**) Quantification of percentage of coverage of PDGFRβ+ pericytes per CD31+ vessels ($n = 3$ mice, all groups). (**F**) Quantification of FITC-dextran+ area per CD31+ vascular area ($n = 3$ mice, all groups). (**G**) Correlation of FITC-dextran leakage and percentage of desmin+ pericyte-covered vessels. Pearson's r correlation coefficient and significance levels are presented ($n = 3$ mice, all groups). (**H** and **I**) Representative images of pimonidazole adduct formation (hypoxyprobe) immunolabeling on FFPE tumor sections (**H**) and corresponding quantification (**I**) of intratumoral hypoxic area as a percentage of tumor area ($n = 3$ mice, all groups). Scale bar: 200 μm. (**J**) Correlation of FITC-dextran leakage and percentage of hypoxic area. Pearson's r correlation coefficient and significance levels are presented. IgG + PBS, $n = 3$; IgG + imatinib, $n = 2$; anti-ANG2 + imatinib, $n = 3$; anti-ANG2 + PBS, $n = 3$; IgG + sunitinib, $n = 3$; anti-ANG2 + sunitinib, $n = 3$. The data are presented as mean ± SD. Unless otherwise indicated, 1-way ANOVA with Tukey's multiple comparison test was used to determine statistical significance. *$P < 0.05$, **$P < 0.01$, ***$P < 0.001$, ****$P < 0.0001$.

3, C and F, and Supplemental Figure 4C). Restored pericyte coverage, notably desmin+ pericyte coverage, strongly associated with reduced vascular leakage (Figure 3, C, F, and G). The increased vascular leakage was strongly correlated with increased intratumoral hypoxia (Figure 3, H–J). While intratumoral hypoxia was vastly enhanced in MDA-MB-231 orthotopic tumors treated with imatinib or sunitinib, the concurrent treatment with anti-Ang2–neutralizing antibodies significantly reduced intratumoral hypoxia levels, a finding which was also observed with anti-Ang2 treatment alone (Figure 3, H and I). Taken together, our results thus support that suppression of Ang2 controlled primary tumor burden with robust remodeling of the angiogenic program, giving rise to tumor vessels with enhanced desmin+ pericyte coverage and reduced vascular leakage, and leading to decreased hypoxia and a reduction in metastatic burden.

Cancer cell control of Ang2 transcriptional activity in endothelial cells defines perivascular heterogeneity. To further define the control of cancer cells on their microenvironmental remodeling, particularly perivascular heterogeneity, we defined the cellular sources of Ang2 in the MDA-MB-321 tumor model and in breast cancer patient–derived xenografts (BCXs) derived from 17 patients (Supplemental Table 4). Presumably, the cellular sources of Ang2 in a growing tumor are predominantly the endothelial cells as well as cancer cells (27). The measure of intratumoral heterogeneity of murine Ang2 expression in resected MDA-MB-231 orthotopic tumors, by excising multiple approximately 1- to 2-mm³ punch biopsies per tumors (Figure 4, A and B), revealed that *Angpt2* expression is significantly correlated with that of endothelial *Pecam1*. These biopsies or tumor cores encompassed various histological representations of the tumors, with variable degrees of necrosis and intratumoral hypoxia, as evidenced by immunolabeling for pimonidazole adduct formation (Figure 4A). Our analyses, using quantitative PCR measurements in each biopsy and primer sequences specific for murine *Angpt2*, showed distinct levels of murine *Angpt2* expression in each specimen evaluated ($n = 4$ mice) (Figure 4B). Murine *Angpt2* expression significantly correlated with endothelial specific *Pecam1* expression (Figure 4B), supporting that endothelial cells are a principle source of Angpt2 transcript, as previously reported (16, 41–43). In the BCXs, similar findings were obtained. The BCX tumors were evaluated for *Angpt2* transcript levels: while human *ANGPT2* transcript levels (cancer cells) were generally low or undetected, with the exception of BCX042 (red dot, Figure 4, C and D), murine *Angpt2* transcript levels were readily detected and further normalized to murine *Pecam1* transcript levels (Figure 4, C and D, and Supplemental Table 4). Notably, BCX042 showed the lowest level of murine *Angpt2* expression (Figure 4D), suggesting that, in this sample, the principal source of Ang2 may be tumor derived rather than host (endothelial cell) derived. The BCXs were extensively characterized: in the 33 BCXs examined, 5 mice representing 3 distinct BCXs showed lung metastases ascertained by histopathological analyses of lung tissue sections (Supplemental Figure 5A and Supplemental Table 4). The sample set evaluated contained BCXs from patients with distinct ER, PR, and HER2 status (Supplemental Table 4). Evaluation of the human *ESR1*, *ESR2*, *PGR*, and *ERBB2* transcript levels in the respective BCX showed measurements consistent with patient primary tumor scoring in a few cases, yet in the majority of cases, the transcript levels were comparable across all BCXs, irrespective of patient primary tumor scoring (Supplemental Figure 5B).

To determine whether the distinct *Angpt2* levels defined the perivascular heterogeneity in the BCX, each tumor section that was stained for CD31, PDGFRβ, desmin, and DAPI was then scanned and subjected to the same automated, vascular, and perivascular phenotyping protocol described above (Figure 1A, Figure
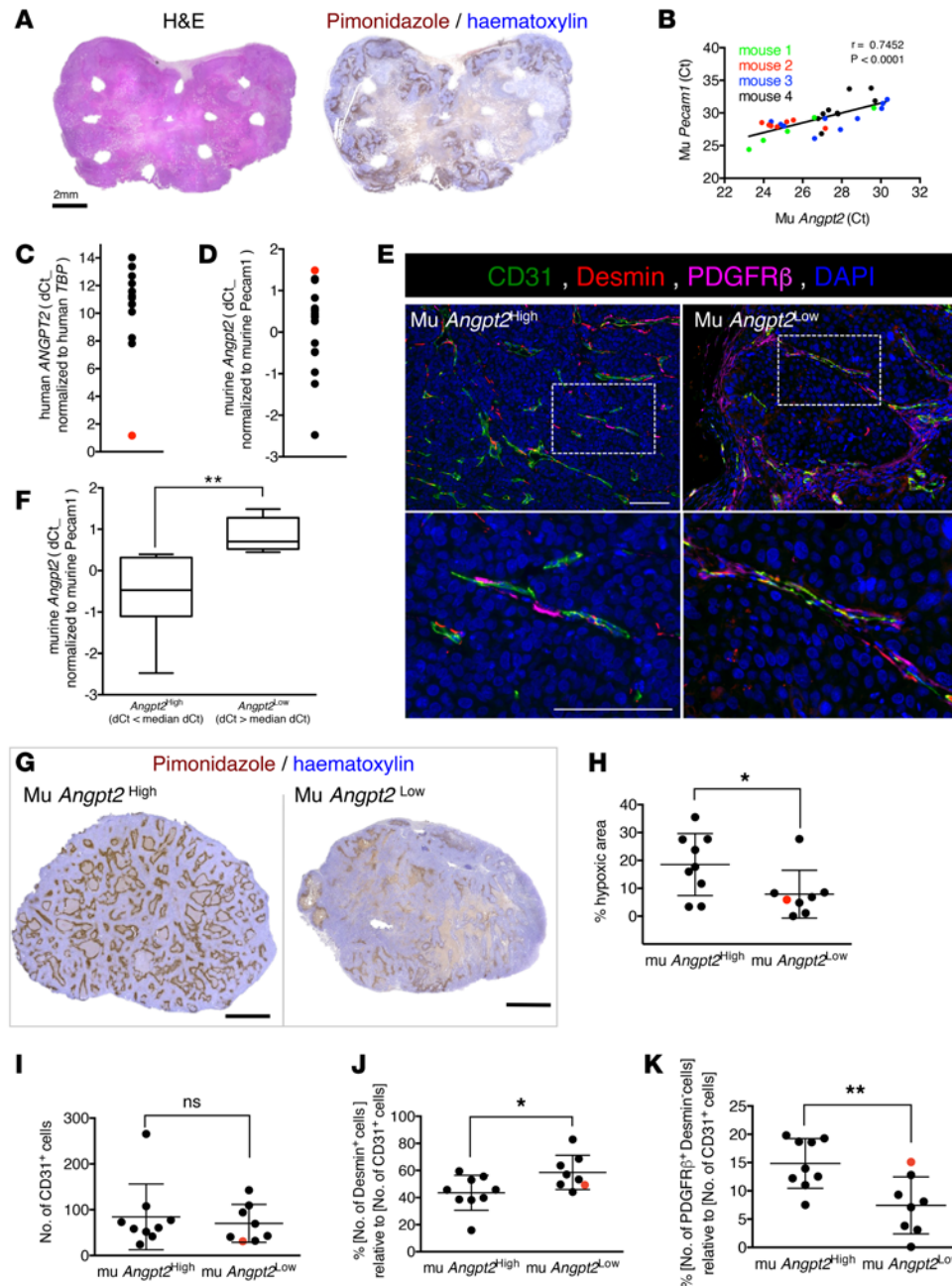
Figure 4. Cancer cell influence on Ang2 expression levels defines vascular integrity in breast cancer patient–derived xenografts. (**A**) H&E staining and immunolabeling of pimonidazole on consecutive sections of MDA-MB-231 tumors implanted in athymic *nu/nu* mice. White areas without tissue correspond to sites where punch biopsies were taken for molecular analysis. Scale bar: 2 mm. (**B**) Correlation of mouse *Angpt2* and *Pecam1* transcript levels on various biopsies obtained from 4 different tumors (*n* = 4 mice). Pearson's r correlation coefficient and significance levels are presented. (**C** and **D**) Analysis of cancer cell–derived human *ANGPT2* and endothelial cell–derived murine *Angpt2* transcript levels in each PDX. Human *ANGPT2* is normalized to human *TBP* (**C**) and murine *Angpt2* (**D**) is normalized to *Pecam1*. Data are presented as dCT. (**E**) Representative images of FFPE tumor sections obtained from murine (mu) *Angpt2*^High^ and mu *Angpt2*^Low^ PDX models immunolabeled for CD31, desmin, and PDGFRβ. The bottom row shows digitally zoomed images. Perivascular cells that have direct contact with CD31⁺ cells and are positive for each marker are quantified. Scale bar: 100 μm. (**F**) Quantification of murine *Angpt2* expression in mu *Angpt2*^High^ and mu *Angpt2*^Low^. Groups are divided based on median value of dCT (Supplemental Table 4). Box-and-whiskers plots show median (line within box), upper and lower quartile (bounds of box), and minimum and maximum values (bars). (**G**) Representative images of pimonidazole immunolabeling of FFPE tumor sections obtained from mu *Angpt2*^High^ and mu *Angpt2*^Low^ PDX models. Scale bar: 2 mm. (**H**) Quantification of the percentage of hypoxic area based on the pimonidazole staining in **G**. (**I**) Quantification of relative vascular density (number of CD31⁺ cells). (**J**) Quantification of the relative percentage of desmin⁺ pericytes associated with CD31⁺ vessels. (**K**) Quantification of the relative percentage of PDGFRβ⁺ desmin⁻ pericytes associated with CD31⁺ vessels. The red dot identifies BCX042 (**C**, **D**, and **H–K**). Experimental *n* numbers were as follows: mu *Angpt2*^High^, *n* = 9; mu *Angpt2*^Low^, *n* = 8. Unless otherwise stated, the data are represented as the mean ± SD, and unpaired 2-tailed *t* test was used to determine statistical significance. *P < 0.05, **P < 0.01.

4E, and Supplemental Figure 6). The BCXs were dichotomized using the median murine *Angpt2* expression to ascertain whether Ang2 expression informed on the perivascular heterogeneity of the tumors (Figure 4F and Supplemental Table 4). Consistent with our studies using MDA-MB-231 orthotopic tumors, which indicated that high Ang2 levels correlated with enhanced intratumoral hypoxia (Figure 3, H and I), BCXs with high *Angpt2* expression presented with significantly higher intratumoral hypoxia (Figure 4, G and H). When comparing the high *Angpt2* and low *Angpt2* groups, we did not observe any differences in overall MVD (Figure 4I). Nonetheless BCXs with high *Angpt2* expression showed markedly reduced desmin⁺ pericyte coverage and increased PDGFRβ⁻desmin⁻ pericyte coverage compared with low *Angpt2* group (Figure 4, J and K). Another independent analysis was carried out using yet another methodology to capture MVD using CD31 label intensity and perivascular heterogeneity using the overlap in CD31 and desmin labels and CD31 and PDGFRβ labels, respectively (Supplemental Figure 5C). The results again indicated that, while we did not observe any differences in overall MVD when comparing high *Angpt2* and low *Angpt2* groups (Supplemental Figure 5D), BCXs with high *Angpt2* expression showed markedly reduced desmin⁺ pericyte coverage (Supplemental Figure 5, E and F), thus confirming the results obtained using perivascular phenotyping (Figure 4, J and K). Ang2 levels thus strongly correlate with the host-derived angiogenic program in BCXs, manifesting itself in distinct pericyte coverage. Such pericyte distribution (low desmin⁺ and high PDGFRβ⁺ pericyte coverage) noted in high *Angpt2* BCXs was similar to that observed in the TNBC patients (cohort 1, Figure 1, D and F–I) as well as patients who received epirubicin monotherapy with poor outcome (cohort 2, Figure 2, D and E, and Supplemental Table 3).

Discussion

The breast tumor microenvironment displays heterogeneous perivascular composition, which affects the angiogenic response and vessel functions in growing tumors. Here, we show that Ang2 critically regulates the perivascular heterogeneity of human breast cancer cell line–derived orthotopic tumors. Specifically, Ang2 promotes perivascular coverage rich in PDGFRβ⁺ cells and poor in desmin⁺ cells, indicative of immature vessels that demonstrated increased permeability and were associated with enhanced intratumoral hypoxia. In support of these observations, gene expression profiling of microdissected breast cancer vascular beds indicated that samples with elevated *ANGPT2* transcripts also showed high levels of *PDGFRB* transcripts (6). While Ang2 protein levels also reflect release from endothelial stores (in Weibel-Palade bodies) upon stimulation, the associated transcriptional upregulation of *Angpt2* supports that increased *Angpt2* transcripts may reflect sustained production of Ang2 and associated signaling response (16, 44). Suppression of Ang2 or low levels of Ang2, in contrast, were associated with a high coverage of desmin⁺ perivascular cells and low coverage of PDGFRβ⁺ cells, and these vessels showed enhanced structural stability, with an effect on diminishing intratumoral hypoxia and suppressing lung metastasis. Our previous studies employing genetically engineered mice to target PDGFRβ⁺ pericytes indicated that anti-Ang2 treatment in this context enhanced desmin⁺ pericyte coverage, resulting in a robust decrease in vascular leakage (16). Inhibition of PDGFRβ⁺ perivascular recruitment using the receptor tyrosine kinase inhibitors sunitinib and imatinib did not increase desmin-rich perivascular coverage, unless combined with anti-Ang2–neutralizing antibodies, indicating that the regulation of heterogeneous perivascular coverage is potently balanced by Ang2-mediated signals. Loss of perivascular cells or PDGFRβ-rich perivascular coverage, unlike desmin-rich perivascular coverage, denoted immature vessels with vulnerable structures and possibly enhanced plasticity and a more sensitive potential for vascular remodeling.

The control of angiogenesis in breast cancer patients has not consistently indicated clinical benefit (45). Notably, in these clinical trials, the combination of agents with antiangiogenic properties and other chemotherapeutic agents may not lend itself to an accurate interpretation of the influence of distinct, preexisting angiogenic programs on the chemotherapy response. Nevertheless, among breast cancer subtypes, TNBC may perhaps respond best to antiangiogenic therapy (46, 47). Our results support this possibility, with tumor vessels in TNBC demonstrating features of immaturity, with limited perivascular coverage or high PDGFRβ⁺/low desmin⁺ perivascular coverage, supporting a destabilized vasculature that is perhaps more responsive to agents targeting, directly or indirectly, tumor angiogenesis. The definition of the tumor perivascular status of TNBC patients may thus offer a useful predictive value to the response to antiangiogenic therapy.

Importantly, our studies indicated that the desmin⁺/PDGFRβ⁺ perivascular ratio predicted the patients' response to epirubicin, with an increase in survival of patients whose tumors presented with high desmin⁺/PDGFRβ⁺ ratio and mature, desmin-rich vessels. In contrast, the desmin⁺/PDGFRβ⁺ perivascular ratio

showed no predictive value for patient response to paclitaxel. While paclitaxel has been proposed to have antiangiogenic activities (48), this proposition is largely supported by in vitro and preclinical studies, and our results, on the basis of perivascular heterogeneity, do not support the pharmacological function of paclitaxel as an indirect angiogenesis inhibitor in breast cancer patients. Neither MVD nor MPI predicted response to paclitaxel. The use of anthracycline chemotherapy, however, was recently demonstrated to inhibit the recruitment of HIF-1 and HIF-1–mediated gene transcription, potentiating a reduction in tumor vascularization (49, 50). *Angpt2* is among the targets of HIF-1 (reviewed in ref. 51), and we postulate that patients with high desmin$^+$/PDGFRβ^+ perivascular ratios would thus further benefit from the indirect effect of epirubicin-mediated suppression of Ang2 production. Thus, patients presenting with high desmin$^+$/low PDGFRβ^+ perivascular coverage could respond more efficiently to epirubicin. Such observations should be tested prospectively in a clinical trial. Although patients with TNBC presented with overall higher MVD and lower MPI compared with non-TNBC patients, there were too few cases in our analyses for definite conclusion on the effect of perivascular composition on the survival of patients with distinct breast cancer subtypes, including TNBC.

Collectively, our data demonstrate that a defined perivascular milieu can inform on breast cancer patient response to epirubicin. These results also potentially delineated a novel understanding of the underlying mechanism of chemotherapeutic intervention using epirubicin given a defined microenvironmental context. We postulate that the level of Ang2 in breast cancer patients could be particularly useful in defining the optimal chemotherapeutic regimen. The context-dependent, multifunctional effects of Ang2 on endothelial cells can also involve several integrins (52, 53), and Ang2/integrin signaling in cancer cells enhances their migration and survival (24). The impact of Ang2 signaling may thus be multipronged, with a direct effect on cancer cell invasive program as well as in tumor immune composition. Indeed, the Ang2/Tie2 signaling influences monocyte functions and tumor immune cell infiltration, with an effect on metastasis (35, 54–56). The combination of specific chemotherapeutic agents with other tumor microenvironment targeted therapies, given a defined perivascular context, may offer yet unforeseen synergistic benefit.

Finally, our studies using PDXs indicated that cancer cells in these xenografts distinctly engaged the host microenvironment, yielding a differential level of host-derived Ang2, perivascular composition, and intratumoral hypoxia. One exception was noted, and in a specific xenograft (BCX042), we found that human *ANGPT2* was the dominant source of Ang2, perhaps highlighting a role for vascular mimicry (57) as yet another level of complexity for perivascular heterogeneity. Our findings using these xenografts support a cancer cell–specific control of the tumor vasculature and perivascular heterogeneity. Cancer cell heterogeneity in tumors from distinct patients with breast cancer, possibly defined by their genomic landscape, may thus distinctly affect vascular co-option and the host angiogenic program. The aggressive features of tumors and their response to therapies may thus emerge via the heterogeneous cancer cell–defined engagement of their microenvironment, including the stimulation and generation of distinct angiogenic programs with a functional effect on disease progression and metastatic dissemination.

Methods

Cells and mice

MDA-MB231 mammary tumor epithelial cells were obtained from MD Anderson's Characterized Cell Line Core Facility and grown in RPMI culture media supplemented with 20% fetal bovine serum. The mycoplasma-free status of all cells was confirmed prior to injection into mice. Eight- to ten-week-old female homozygous athymic nude mice were purchased from Charles River Laboratories. MDA-MB-231 cells were implanted orthotopically and bilaterally (0.5×10^6 in each mammary fat pad) into 8- to 10-week-old female nude mice. Tumor volumes were measured every 2 to 3 days using Vernier calipers, and volumes were calculated using the formula (length × width^2 × π/6). Mice were randomized when the average tumor burden reached 500 mm^3 and treated with imatinib, sunitinib, or PBS (control) by oral gavage daily (50 mg/kg BW in 0.1 ml). Mice also received an i.p. injection of the neutralizing anti-Ang2 antibody (LC06, Roche Pharma Research and Early Development) or control isotype-matched IgG antibody once a week (10 mg/kg BW in 0.2 ml PBS) (40). All mice were injected i.p. with a single dose of hypoxyprobe (HPI Inc.; 60 mg/kg BW in 0.5 ml of PBS) 30 minutes before euthanasia. Mice were euthanized when the tumor size of control mice reached approximately 2,500 mm^3.

PDX

The methodology to generate the PDX (also referred to herein as the BCX) has been previously described (58). Briefly, surgically resected breast tumors were cut into 3-mm^3 fragments and inserted into the subcutaneous space on the flank or mammary gland of immune-deficient mice. Tumors that successfully engrafted were serial transplanted to additional mice following the same procedure. Tumor size was measured at euthanasia using Vernier calipers, and tumor and lung tissues were processed as described below.

Patient cohorts

Cohort 1. Samples from human TNBC patients ($n = 28$, $n = 7$ treatment naive) and luminal breast cancer patients ($n = 57$, $n = 16$ treatment naive) were retrieved from the Anatomic Pathology Department of the AC Camargo Cancer Center. The formalin-fixed paraffin-embedded (FFPE) samples were punched and included in a TMA for further immunohistochemical assessments.

Cohort 2. Pretreatment incisional tumor biopsies were available from patients with locally advanced breast cancer (T3/T4 and/or N2/N3) included in the neoadjuvant phase II EpiTax trial, Bergen, Norway (37, 38). Briefly, patients were randomized to either epirubicin 90 mg/m^2 or paclitaxel 200 mg/m^2 q3w, administered in 4 to 6 courses. Patients with suboptimal tumor response to either drug switched to the opposite chemotherapy regimen. Response rates (according to the UICC criteria) and breast cancer characteristics were previously reported (23, 37, 38). Follow-up data were available for >10 years or up to time of death for all patients in the trials. For the current analysis, FFPE tumor tissue was available from 144 patients as TMAs, with corresponding response evaluation data; breast cancer characteristics, including TNM status; and survival data (Supplemental Table 2).

Quantification of metastatic burden and tumor necrosis

Four-μm-thick sections of FFPE lung tissue were stained with H&E. Microscopic images of the entire lobe of each lung were obtained using the Aperio Slide Scanner. Metastases were identified via histopathological analysis of H&E-stained lung sections, and metastatic areas were quantified, using Pannoramic Viewer software (3DHISTECH Ltd.), as a percentage of total lung area. Except for one mouse, for which the lung tissue was too poor a quality to determine metastatic disease accurately, all mice were evaluated. High-magnification images (original magnification, ×100 or ×90) of the metastatic area are provided for each lung photomicrograph. Metastases were also identified on FFPE lung sections by Ki67 immunohistochemistry staining. Necrotic tumor area was assessed on H&E-stained sections of the entire tumor and was quantified, using Pannoramic Viewer software (3DHISTECH Ltd.), as a percentage of total tumor area.

Tumor vessel leakage

Mice were injected in the retro-orbital venous plexus with 100 μl of 10 mg/ml FITC-dextran (2,000,000 MW, Sigma-Aldrich) 10 minutes before euthanasia. Fresh frozen sections from O.C.T. embedded tumors were immunostained for CD31. CD31 and FITC-dextran were then visualized directly by fluorescent microscopy under the red and green fluorescent filters, respectively. The resulting fluorescent images were quantified using the NIH ImageJ analysis software, and data are presented as FITC-dextran–positive area normalized by CD31-positive area. Multiple sections/tumor were analyzed at an original magnification of ×40, with $n \geq 3$ tumors/group.

Immunostaining

Tumors and lungs were fixed in 10% neutral buffered formalin and processed for paraffin embedding. Five-μm sections were obtained from FFPE tissue and used for immunostaining. For hypoxyprobe immunohistochemistry, the deparaffinized tumor sections were incubated in heated 10 mM citrate buffer (pH 6.0) for 15 minutes (EZ Retriever microwave, BioGenex) prior to blocking with M.O.M. Mouse IgG Blocking Reagent (Vector Laboratories) for 1 hour. Immunostaining was performed as described previously (16). Whole-tumor images were obtained using the Aperio Slide Scanner, and DAB-positive (brown) staining was analyzed by NIH ImageJ analysis software on scanned tumor images. Consecutive unstained sections on the same slide served as negative controls (no primary antibody) and were used to subtract background. Control and treated mice within an experimental set (3 or more tumors/group) were analyzed, and results are reported as staining area per tumor section.

For all other stainings, FFPE sections were incubated in heated TE buffer (pH 9.0) for 30 minutes (EZ Retriever microwave, BioGenex) for antigen retrieval. Sections were blocked for 1 hour with 4% cold water fish gelatin (CWFG) in phosphate-buffered saline w/Tween 20 (PBST) at room temperature. Following blocking, sections were incubated in 1:50 rat anti-CD31 (Dianova, DIA310), 1:100 rabbit anti-PDGFRβ (Thermo, MA5-15143), 1:50 mouse anti-desmin (Sigma-Aldrich, D1033), or 1:400 rabbit anti-Ki67 (Thermo, RM-9106-S1) at 4°C overnight, followed by 1 hour of incubation with fluorescent secondary antibodies. Slides were mounted with Fluoroshield mounting medium. Positive staining was quantified in ≥6 visual fields/tumor at an original magnification of ×40 using NIH ImageJ analysis software, where the same threshold was used for all compared conditions to determine the fraction of positive staining area per field. At least 3 tumors/group were used in the assessments. Stainings were visualized on either a Zeiss Axio Observer A1 inverted microscope or a Zeiss LSM 510 Meta Confocal microscope. The number of vessels associated with pericytes was determined using the ImageJ cell counter application under an original magnification of ×40 and was reported as the percentage of vessels that were associated with pericytes per the total number of vessels per visual field.

Four-color immunohistochemical multiplex

Five-μm-thick sections of FFPE TMA blocks were deparaffinized, rehydrated, and refixed with formaldehyde/methanol (1:10) prior to antigen retrieval in heated TE buffer (pH 9.0) for 30 minutes (EZ Retriever microwave, BioGenex). Each TMA section was sequentially stained for 3 different antibodies, each round of staining including a blocking step with 4% CWFG in TBST followed by primary antibody incubation and corresponding secondary HRP-conjugated polymer (SuperPicture, Invitrogen). Each HRP-conjugated polymer mediated the covalent binding of a different fluorophore (FITC, Cy3, and Cy5) using Tyramide Signal Amplification (PerkinElmer). This covalent reaction was followed by additional antigen retrieval in heated citric acid buffer (pH 6.0) for 15 minutes to remove bound antibodies before the next step in the sequence, which allows for the use of multiple primary antibodies with the same species origin. After all 3 sequential reactions, sections were counterstained with DAPI (Life Technologies) and mounted with VECTASHIELD Antifade Mounting Medium (Vector Laboratories). Primary antibodies were used for this protocol as follows: rabbit anti-CD31 (1:4,000, Bethyl Laboratories, IHC-00055), rabbit anti-PDGFRβ (1:300, Thermo, MA5-15143), and mouse anti-desmin (1:100, Sigma-Aldrich, D1033).

Multispectral image analysis, spectral unmixing, and phenotyping

Images were obtained on a Vectra multispectral microscope (Perkin-Elmer) using DAPI (440 nm to 680 nm), FITC (520 nm to 680 nm), Cy3 (570 nm to 690 nm), Texas Red (580 nm to 700 nm), and Cy5 (670 nm to 720 nm) filter cubes. Stained slides were imaged every 10 nm within the range of each filter to generate multispectral images. Four individual ×200 multispectral images were obtained per core and stitched together to form a final multispectral image per TMA core. For the BCX tumor sections, 15 to 45 images were obtained per tumor. Multispectral images were subsequently analyzed using the InForm image analysis software (Perkin-Elmer), where a spectral library was generated based on the individual spectral properties on each fluorophore used as well as autofluorescence information obtained from the imaged slides (Supplemental Figure 1A). All images were spectrally unmixed into their individual fluorescent components, with each individual cell identified based on the DAPI stain. All images were then segmented into three individual regions (blank, pericellular, and other) using an InForm segmentation algorithm based on the CD31 and DAPI staining intensities (Figure 1A). Individually identified cells within the perivascular region were finally subjected to a proprietary InForm active learning phenotyping algorithm, where the spectral information as well as shape/size features were used to assign each cell a previously determined phenotype (Figure 1A and Supplemental Figure 1B). Using this methodology, all cells within the perivascular regions of each core were phenotyped into one of the following classes: endothelial cells/blood vessels (CD31$^+$); desmin$^+$ pericytes (CD31$^-$, desmin$^+$, PDGFRβ$^-$); PDGFRβ$^+$ pericytes (CD31$^-$, desmin$^-$, PDGFRβ$^+$); desmin$^+$ PDGFRβ$^+$ pericytes (CD31$^-$, desmin$^+$, PDGFRβ$^+$); and other (CD31$^-$, desmin$^-$, PDGFRβ$^-$).

MVD and MPI quantification

MVD is presented as the total number of nuclei associated with CD31$^+$ positivity per core. Total pericyte coverage defining the MPI is calculated using the following formula: Σ (PDGFRβ$^-$desmin$^+$ cells + PDGFRβ$^+$desmin$^-$ cells + PDGFRβ$^+$desmin$^+$ cells)/CD31$^+$ cells × 100 per core. In some cases, pericytes counts

exceeded the endothelial cell count (Figure 1, C and F), because, depending on plane of view, not all CD31^{+} cell nuclei are captured despite positive CD31 membrane staining, hence resulting pericyte coverage greater than 100%. This did not affect the segmentation analysis since segmentation process was based on CD31 positivity on the membrane. The relative pericyte distribution (Figure 1, D and E) was presented as follows: the naked vessels (black bars) were defined as 100 (chosen arbitrarily) minus MPI (expressed as a percentage). The remaining vessels (covered by pericyte type: green, yellow, or red bars) were then computed to show the relative distribution of PDGFRβ^{–}desmin^{+}/CD31^{+}, PDGFRβ^{+}desmin^{–}/CD31^{+}, and PDGFRβ^{+}desmin^{+}/CD31^{+} ratios over a scale of 100 (also chosen arbitrarily).

Colocalization analysis of pericyte coverage

Multispectral images of 4-color multiplexed FFPE sections obtained from PDX tumor tissue were also subjected to colocalization analysis. In this method, pixel numbers from overlapping areas between CD31^{+} (endothelial cells) and desmin^{+} (pericytes) or CD31^{+} (endothelial cells) and PDGFRβ^{+} (pericyte) were measured on the InForm image analysis software (Perkin-Elmer). With colocalization methods, only tight associations between endothelial cells and pericytes were measured, as the software could only detect the overlap of two different fluorophores.

Quantitative PCR analyses

Total RNA was isolated from MDA-MB-231 tumor cores from punch biopsies ($n = 4$) or PDX tumors ($n = 17$) using TRIzol Reagent (Invitrogen) following the manufacturer's directions. 2 μg of total RNA was used to synthesize cDNA using the High-Capacity cDNA Reverse Transcription Kit (Applied Biosystems). Diluted cDNA from MDA-MB-231 tumors was amplified using Power SYBR Green PCR Master Mix (Applied Biosystems) and the following primers: *Angpt2* forward 5′-AGCAGATTTTGGAT-CAGACCAG-3′, *Anptg2* reverse 5′-GCTCCTTCATGGACTGTAGCTG-3′, *Pecam1* forward 5′-ACGCT-GGTGCTCTATGCAAG-3′, and *Pecam1* reverse 5′-TCAGTTGCTGCCCATTCATCA.

qRT-PCR for PDX tumor samples was performed using a TaqMan Gene Expression Assay system (Applied Biosystems). Diluted cDNA was amplified using a TaqMan Gene Expression Master Mix (Applied Biosystems) and the following gene expression assay: *PGR* (Hs01556702_m1), *ERBB2* (Hs01001580_m1), h*ANGPT2* (Hs00169867_m1), m*Angpt2* (Mm00545822_m1), m*Pecam1* (Mm01242576_m1), *ESR1* (Hs01046818_m1), *ESR2* (Hs00230957_m1), h*RPLP0* (Hs99999902_m1), and h*TBP* (Hs00427621_m1).

ELISA

Blood samples were collected into heparin-containing tubes and spun down for 10 minutes at 4,000 *g* at 4°C. Plasma was collected and stored at –20°C until use. Serial dilutions of plasma were tested for optimal protein concentration. Plasma samples were diluted in sample diluent buffer provided with the Angiopoietin-2 Mouse ELISA Kit (Abcam, ab171335), and the ELISA was then carried out following manufacturer's directions.

Statistics

All statistical analyses were performed using the GraphPad Prism statistical analysis software. For comparison between two groups with one grouping variable, the unpaired 2-tailed Student's *t* test was used. To compare multiple groups with one grouping variable, 1-way ANOVA with Tukey's multiple comparison test was performed. To compare multiple groups with two grouping variables, 2-way ANOVA with Sidak's multiple comparison test was used. For survival analysis, Kaplan-Meier curves were drawn and differences between the curves were established using the log-rank test. For correlation analysis, Pearson's correlation coefficient was calculated using GraphPad Prism. Data are presented as the mean, with error bars corresponding to SD, and/or as dot plots for representation of individual *n* values. Box-and-whiskers plots show median (line within box), upper and lower quartile (bounds of box), and minimum and maximum values (bars). $P < 0.05$ was considered statistically significant.

Study approval

Animal. All animal studies were reviewed and approved by the Institute of Animal Care and Use Committee at the MD Anderson Cancer Center.

Cohort 1. Samples were retrieved from the Anatomic Pathology Department of the AC Camargo Cancer Center, and this study was approved by the Ethical Committee of the A C Camargo Cancer Center (process 1655/12). All patients have provided informed consent.

Cohort 2. The study protocols were approved by the Regional Committee for Medical and Health Research Ethics West (Norway), reference 030.06. All patients had provided informed consent before inclusion in the protocols, which included future studies on prognostic and predictive factors.

Author contributions

VSL conceptually designed the strategy for this study, participated in discussions, provided intellectual input, supervised the studies, designed and performed experiments, and wrote the manuscript. JK provided intellectual input and supervised the studies. JK and PCS designed and performed experiments, collected the data, generated the figures, and participated in writing the manuscript. DML, QP, KWE, HS, MG, and NSA performed some experiments and collected data. The data were analyzed by JK, VSL, and PCS. YK provided reagents. RMR, HPE, PEL, and FMB provided samples, participated in discussion, provided intellectual input, and edited the manuscript.

Address correspondence to: Valerie LeBleu, Department of Cancer Biology, University of Texas MD Anderson Cancer Center, 1881 East Road, Unit 1906, Houston, Texas 77054, USA. Phone: 713.792.7915; E-mail: vlebleu@mdanderson.org.

1. Li YJ, et al. Perfusion heterogeneity in breast tumors for assessment of angiogenesis. *J Ultrasound Med*. 2013;32(7):1145–1155.
2. Eberhard A, Kahlert S, Goede V, Hemmerlein B, Plate KH, Augustin HG. Heterogeneity of angiogenesis and blood vessel maturation in human tumors: implications for antiangiogenic tumor therapies. *Cancer Res*. 2000;60(5):1388–1393.
3. Cooke VG, et al. Pericyte depletion results in hypoxia-associated epithelial-to-mesenchymal transition and metastasis mediated by met signaling pathway. *Cancer Cell*. 2012;21(1):66–81.
4. Smith MJ, Berger RW, Minhas K, Moorehead RA, Coomber BL. Heterogeneity of vascular and progenitor cell compartments in tumours from MMTV-PyVmT transgenic mice during mammary cancer progression. *Int J Exp Pathol*. 2011;92(2):106–116.
5. Senchukova MA, Nikitenko NV, Tomchuk ON, Zaitsev NV, Stadnikov AA. Different types of tumor vessels in breast cancer: morphology and clinical value. *Springerplus*. 2015;4:512.
6. Pepin F, et al. Gene-expression profiling of microdissected breast cancer microvasculature identifies distinct tumor vascular subtypes. *Breast Cancer Res*. 2012;14(4):R120.
7. Armulik A, Genové G, Betsholtz C. Pericytes: developmental, physiological, and pathological perspectives, problems, and promises. *Dev Cell*. 2011;21(2):193–215.
8. Edelman DA, Jiang Y, Tyburski J, Wilson RF, Steffes C. Pericytes and their role in microvasculature homeostasis. *J Surg Res*. 2006;135(2):305–311.
9. Gerhardt H, Semb H. Pericytes: gatekeepers in tumour cell metastasis? *J Mol Med*. 2008;86(2):135–144.
10. Meng MB, et al. Pericytes: a double-edged sword in cancer therapy. *Future Oncol*. 2015;11(1):169–179.
11. Raza A, Franklin MJ, Dudek AZ. Pericytes and vessel maturation during tumor angiogenesis and metastasis. *Am J Hematol*. 2010;85(8):593–598.
12. von Tell D, Armulik A, Betsholtz C. Pericytes and vascular stability. *Exp Cell Res*. 2006;312(5):623–629.
13. Huang Y, Goel S, Duda DG, Fukumura D, Jain RK. Vascular normalization as an emerging strategy to enhance cancer immunotherapy. *Cancer Res*. 2013;73(10):2943–2948.
14. Jain RK. A new target for tumor therapy. *N Engl J Med*. 2009;360(25):2669–2671.

15. Kerbel RS, Viloria-Petit A, Klement G, Rak J. 'Accidental' anti-angiogenic drugs. *Eur J Cancer*. 2000;36(10):1248–1257.

16. Keskin D, et al. Targeting vascular pericytes in hypoxic tumors increases lung metastasis via angiopoietin-2. *Cell Rep*. 2015;10(7):1066–1081.

17. Xian X, et al. Pericytes limit tumor cell metastasis. *J Clin Invest*. 2006;116(3):642–651.

18. Augustin HG, Koh GY, Thurston G, Alitalo K. Control of vascular morphogenesis and homeostasis through the angiopoietin-Tie system. *Nat Rev Mol Cell Biol*. 2009;10(3):165–177.

19. Eklund L, Saharinen P. Angiopoietin signaling in the vasculature. *Exp Cell Res*. 2013;319(9):1271–1280.

20. Saharinen P, et al. Angiopoietins assemble distinct Tie2 signalling complexes in endothelial cell-cell and cell-matrix contacts. *Nat Cell Biol*. 2008;10(5):527–537.

21. Thomas M, Augustin HG. The role of the Angiopoietins in vascular morphogenesis. *Angiogenesis*. 2009;12(2):125–137.

22. Scharpfenecker M, Fiedler U, Reiss Y, Augustin HG. The Tie-2 ligand angiopoietin-2 destabilizes quiescent endothelium through an internal autocrine loop mechanism. *J Cell Sci*. 2005;118(pt 4):771–780.

23. Eikesdal HP, Knappskog S, Aas T, Lønning PE. TP53 status predicts long-term survival in locally advanced breast cancer after primary chemotherapy. *Acta Oncol*. 2014;53(10):1347–1355.

24. Imanishi Y, et al. Angiopoietin-2 stimulates breast cancer metastasis through the α(5)β(1) integrin-mediated pathway. *Cancer Res*. 2007;67(9):4254–4263.

25. Avraham HK, Jiang S, Fu Y, Nakshatri H, Ovadia H, Avraham S. Angiopoietin-2 mediates blood-brain barrier impairment and colonization of triple-negative breast cancer cells in brain. *J Pathol*. 2014;232(3):369–381.

26. Rigamonti N, Kadioglu E, Keklikoglou I, Wyser Rmili C, Leow CC, De Palma M. Role of angiopoietin-2 in adaptive tumor resistance to VEGF signaling blockade. *Cell Rep*. 2014;8(3):696–706.

27. Sfiligoi C, et al. Angiopoietin-2 expression in breast cancer correlates with lymph node invasion and short survival. *Int J Cancer*. 2003;103(4):466–474.

28. Li P, He Q, Luo C, Qian L. Diagnostic and prognostic potential of serum angiopoietin-2 expression in human breast cancer. *Int J Clin Exp Pathol*. 2015;8(1):660–664.

29. Holopainen T, et al. Effects of angiopoietin-2-blocking antibody on endothelial cell-cell junctions and lung metastasis. *J Natl Cancer Inst*. 2012;104(6):461–475.

30. Imanishi Y, Hu B, Xiao G, Yao X, Cheng SY. Angiopoietin-2, an angiogenic regulator, promotes initial growth and survival of breast cancer metastases to the lung through the integrin-linked kinase (ILK)-AKT-B cell lymphoma 2 (Bcl-2) pathway. *J Biol Chem*. 2011;286(33):29249–29260.

31. Srivastava K, et al. Postsurgical adjuvant tumor therapy by combining anti-angiopoietin-2 and metronomic chemotherapy limits metastatic growth. *Cancer Cell*. 2014;26(6):880–895.

32. Tsutsui S, et al. Angiopoietin 2 expression in invasive ductal carcinoma of the breast: its relationship to the VEGF expression and microvessel density. *Breast Cancer Res Treat*. 2006;98(3):261–266.

33. Gerald D, Chintharlapalli S, Augustin HG, Benjamin LE. Angiopoietin-2: an attractive target for improved antiangiogenic tumor therapy. *Cancer Res*. 2013;73(6):1649–1657.

34. Mazzieri R, et al. Targeting the ANG2/TIE2 axis inhibits tumor growth and metastasis by impairing angiogenesis and disabling rebounds of proangiogenic myeloid cells. *Cancer Cell*. 2011;19(4):512–526.

35. Rigamonti N, De Palma M. A role for angiopoietin-2 in organ-specific metastasis. *Cell Rep*. 2013;4(4):621–623.

36. Tolaney SM, et al. Role of vascular density and normalization in response to neoadjuvant bevacizumab and chemotherapy in breast cancer patients. *Proc Natl Acad Sci U S A*. 2015;112(46):14325–14330.

37. Chrisanthar R, et al. CHEK2 mutations affecting kinase activity together with mutations in TP53 indicate a functional pathway associated with resistance to epirubicin in primary breast cancer. *PLoS One*. 2008;3(8):e3062.

38. Chrisanthar R, et al. Predictive and prognostic impact of TP53 mutations and MDM2 promoter genotype in primary breast cancer patients treated with epirubicin or paclitaxel. *PLoS One*. 2011;6(4):e19249.

39. Knappskog S, et al. Concomitant inactivation of the p53- and pRB- functional pathways predicts resistance to DNA damaging drugs in breast cancer in vivo. *Mol Oncol*. 2015;9(8):1553–1564.

40. Thomas M, et al. A novel angiopoietin-2 selective fully human antibody with potent anti-tumoral and anti-angiogenic efficacy and superior side effect profile compared to Pan-Angiopoietin-1/-2 inhibitors. *PLoS One*. 2013;8(2):e54923.

41. Gale NW, et al. Angiopoietin-2 is required for postnatal angiogenesis and lymphatic patterning, and only the latter role is rescued by Angiopoietin-1. *Dev Cell*. 2002;3(3):411–423.

42. Hansen TM, Singh H, Tahir TA, Brindle NP. Effects of angiopoietins-1 and -2 on the receptor tyrosine kinase Tie2 are differentially regulated at the endothelial cell surface. *Cell Signal*. 2010;22(3):527–532.

43. Hegen A, Koidl S, Weindel K, Marmé D, Augustin HG, Fiedler U. Expression of angiopoietin-2 in endothelial cells is controlled by positive and negative regulatory promoter elements. *Arterioscler Thromb Vasc Biol*. 2004;24(10):1803–1809.

44. Fiedler U, et al. The Tie-2 ligand angiopoietin-2 is stored in and rapidly released upon stimulation from endothelial cell Weibel-Paladebodies. *Blood*. 2004;103(11):4150–4156.

45. Mackey JR, et al. Controlling angiogenesis in breast cancer: a systematic review of anti-angiogenic trials. *Cancer Treat Rev*. 2012;38(6):673–688.

46. Sikov WM, et al. Impact of the addition of carboplatin and/or bevacizumab to neoadjuvant once-per-week paclitaxel followed by dose-dense doxorubicin and cyclophosphamide on pathologic complete response rates in stage II to III triple-negative breast cancer: CALGB 40603 (Alliance). *J Clin Oncol*. 2015;33(1):13–21.

47. von Minckwitz G, et al. Neoadjuvant chemotherapy and bevacizumab for HER2-negative breast cancer. *N Engl J Med*. 2012;366(4):299–309.

48. Bocci G, Di Paolo A, Danesi R. The pharmacological bases of the antiangiogenic activity of paclitaxel. *Angiogenesis*. 2013;16(3):481–492.

49. Lee K, Qian DZ, Rey S, Wei H, Liu JO, Semenza GL. Anthracycline chemotherapy inhibits HIF-1 transcriptional activity and tumor-induced mobilization of circulating angiogenic cells. *Proc Natl Acad Sci U S A*. 2009;106(7):2353–2358.

50. Tanaka T, Yamaguchi J, Shoji K, Nangaku M. Anthracycline inhibits recruitment of hypoxia-inducible transcription factors and

suppresses tumor cell migration and cardiac angiogenic response in the host. *J Biol Chem*. 2012;287(42):34866–34882.

51. Liu W, Shen SM, Zhao XY, Chen GQ. Targeted genes and interacting proteins of hypoxia inducible factor-1. *Int J Biochem Mol Biol*. 2012;3(2):165–178.

52. Felcht M, et al. Angiopoietin-2 differentially regulates angiogenesis through TIE2 and integrin signaling. *J Clin Invest*. 2012;122(6):1991–2005.

53. Hakanpaa L, et al. Endothelial destabilization by angiopoietin-2 via integrin β1 activation. *Nat Commun*. 2015;6:5962.

54. Coffelt SB, et al. Angiopoietin 2 stimulates TIE2-expressing monocytes to suppress T cell activation and to promote regulatory T cell expansion. *J Immunol*. 2011;186(7):4183–4190.

55. De Palma M, Naldini L. Angiopoietin-2 TIEs up macrophages in tumor angiogenesis. *Clin Cancer Res*. 2011;17(16):5226–5232.

56. Coffelt SB, et al. Angiopoietin-2 regulates gene expression in TIE2-expressing monocytes and augments their inherent proangiogenic functions. *Cancer Res*. 2010;70(13):5270–5280.

57. Wagenblast E, et al. A model of breast cancer heterogeneity reveals vascular mimicry as a driver of metastasis. *Nature*. 2015;520(7547):358–362.

58. McAuliffe PF, et al. Ability to generate patient-derived breast cancer xenografts is enhanced in chemoresistant disease and predicts poor patient outcomes. *PLoS One*. 2015;10(9):e0136851.